Journal of Power Sources 300 (2015) 413–418

Contents lists available at ScienceDirect

Journal of Power Sources

journal homepage: www.elsevier.com/locate/jpowsour

Reversible lithium intercalation in a lithium-rich layered rocksalt Li_2RuO_3 cathode through a Li_3PO_4 solid electrolyte

Yueming Zheng [a], Masaaki Hirayama [a, *], Sou Taminato [a], Soyeon Lee [b, c], Yoshifumi Oshima [c, d], Kunio Takayanagi [c, e], Kota Suzuki [a], Ryoji Kanno [a]

[a] Department of Electronic Chemistry, Interdisciplinary Graduate School of Science and Engineering, Tokyo Institute of Technology, 4259 Nagatsuta, Midori-ku, Yokohama, 226-8502, Japan
[b] Quantum Nanoelectronics Research Center, Tokyo Institute of Technology, 2-12-1-H-51 Oh-okayama, Meguro-ku, Tokyo, 152-8551, Japan
[c] JST-CREST, 7-Gobancho, Chiyoda-ku, Tokyo, 102-0075, Japan
[d] School of Materials Science I, Japan Advanced Institute of Science and Technology, 1-1 M1-61, Asahidai, Nomi, Ishikawa, 923-1292, Japan
[e] Department of Physics, Tokyo Institute of Technology, 2-12-1-H-51 Oh-okayama, Meguro-ku, Tokyo, 152-8551, Japan

HIGHLIGHTS

- All-solid-state batteries of Li(In)/Li_3PO_4/Li_2RuO_3(001) were fabricated.
- The batteries delivered highly-reversible (de)intercalation during the 30 cycles.
- The rate capability of the battery was comparable to that of a liquid-type battery.

ARTICLE INFO

Article history:
Received 1 June 2015
Received in revised form
17 September 2015
Accepted 25 September 2015
Available online xxx

Keywords:
All-solid-state battery
Thin-film battery
Lithium ruthenium oxide
Lithium rich layered oxide
Pulsed laser deposition

ABSTRACT

Li_2RuO_3 (001) films with a lithium-rich layered rocksalt structure are epitaxially grown on a Al_2O_3(0001) substrate through pulsed laser deposition, followed by stacking of an amorphous Li_3PO_4 solid electrolyte. A half solid-state battery with a Li_3PO_4/Li_2RuO_3 cathode, liquid electrolyte, and lithium anode exhibits two redox peak pairs at 3.4 and 3.6 V, demonstrating lithium intercalation in the Li_2RuO_3 through the Li_3PO_4 solid electrolyte. All-solid-state batteries are fabricated by Li or In metal anode deposition on the Li_3PO_4/Li_2RuO_3. The Li/Li_3PO_4/Li_2RuO_3 cell delivers an initial discharge capacity of 101 mAh g^{-1}, which does not fade significantly over 30 cycles. Furthermore, the Li_2RuO_3 rate capability is comparable to that of a liquid-type battery. Lithium-rich layered materials are available for use as cathodes in all-solid-state batteries.

© 2015 Elsevier B.V. All rights reserved.

1. Introduction

All-solid-state lithium batteries are attracting significant attention due to their inherent safety and high volumetric energy density compared to traditional lithium–ion batteries [1]. Various cathode materials, such as $LiCoO_2$ [2,3], Li(Ni,Co)O_2 [4,5], $LiMn_xNi_{2-x}O_4$ [6,7], and $LiFePO_4$ [8], were reported as electrochemically active with oxide-type solid electrolytes composed of Li_3PO_4 [9] or $Li_3PO_xN_y$ [6]. Among these materials, $LiCoO_2$ with a layered rocksalt structure exhibits a highly reversible intercalation reaction in an all-solid-state battery [2]. However, the associated charge/discharge capacity is intrinsically low (125 mAh g^{-1}) due to the low quantity of possible lithium sites in the crystal structure. Recently, lithium-rich layered materials with much higher theoretical capacities of over 200 mAh g^{-1}, including Li_2MO_3 [10–14] and Li[Li,M]O_2 [15–19] (M = 3d and 4d transition metals), were recognized as promising intercalation cathodes for lithium batteries using organic liquid electrolytes. These lithium-rich layered materials have a similar crystal structure to $LiCoO_2$, consisting of oxide ions in cubic close packing and the basal planes of the octahedral interstices filled by 1/3 Li and 2/3M ions. The lithium ions in the MO_6 layers can participate in the intercalation reaction [20], leading to the high theoretical capacity of these materials. However, until date, there are no reports concerning the application of

* Corresponding author.
E-mail address: hirayama@echem.titech.ac.jp (M. Hirayama).

http://dx.doi.org/10.1016/j.jpowsour.2015.09.097
0378-7753/© 2015 Elsevier B.V. All rights reserved.

these lithium-rich layered materials as cathodes in all-solid-state batteries.

Here, we report the lithium intercalation properties of the lithium-rich layered material Li_2RuO_3 combined with the solid electrolyte Li_3PO_4 using an epitaxial model system. Among the various materials with a lithium-rich layered rocksalt structure, Li_2RuO_3 shows highly reversible lithium intercalation with no significant structural alterations in liquid battery systems [10]. Therefore, this material is a suitable cathode for the investigation of the lithium intercalation properties of lithium-rich layered materials in all-solid-state batteries. In the present study, we fabricate a solid–solid interface composed of an epitaxial-film cathode made of Li_2RuO_3 (001), deposited by pulsed laser deposition (PLD), with an amorphous Li_3PO_4 film as the electrolyte. The structure and lithium intercalation properties of the solid–solid interface are investigated by X-ray diffraction (XRD), hard X-ray photoemission spectroscopy (HAXPES), and electrochemical cyclic voltammetry. All-solid-state In/Li_3PO_4/Li_2RuO_3 and Li/Li_3PO_4/Li_2RuO_3 thin film batteries are also fabricated, and their performance is characterized by electrochemical charge/discharge measurements.

2. Experimental

Epitaxial Li_2RuO_3(001) thin films were grown on Al_2O_3(0001) substrates using a 248 nm KrF excimer laser in conjunction with a PLD apparatus (PLAD131, AOV, Inc.), according to the experimental conditions described previously [20,21]. The Li_3PO_4 solid electrolyte was deposited on the epitaxial Li_2RuO_3 film by radiofrequency (RF) magnetron sputtering (PSAD-3000, AOV, Inc) using a stoichiometric Li_3PO_4 target (ϕ 50 mm × 4 mmt, Toshima Manufacturing Co., Ltd), under the following conditions: distance between the target and the substrate = 30 mm, temperature = 298 K, gas pressure = 0.48 Pa, O_2/Ar (4:1) flow, and power = 100 W. The crystal structures and orientations of the films were characterized by out-of-plane and in-plane XRD analyses with Cu Kα_1 radiation (Rigaku, ATX-G). The thicknesses and morphologies of the films were assessed by thin-film stylus profilometry (Bruker, DektakXT). The Li_3PO_4 films ionic conductivity was determined by electrochemical impedance spectroscopy (Solartron, 1260 and 1289) with gold current collectors deposited on both sides of a 2-μm-thick Li_3PO_4 film.

Preliminary characterization of the solid–solid interface was performed by cyclic voltammetry measurements on a half-cell consisting of a Li_3PO_4/Li_2RuO_3 film cathode, an organic liquid electrolyte, and a Li metal anode. The liquid electrolyte was ethylene carbonate/diethyl carbonate (3:7) containing 1 mol dm^{-3} $LiPF_6$. The Li_2RuO_3 film structural changes before and after electrochemical reactions were examined by HAXPES. The HAXPES data were collected using a hemispherical electron–energy analyzer (BL46XU at SPring-8, Japan) applying an excitation energy of 7938.9 eV. The HAXPES spectra were normalized by the carbon binding energy (280.7 eV) and the area of the respective elemental signals.

All-solid-state batteries were fabricated by In or Li anode stacking on the Li_3PO_4/Li_2RuO_3 films using the vacuum vapor-deposition method (ALS Technology, E–80Li). The chamber was evacuated to a base pressure below 8×10^{-4} Pa, and the In and Li films were grown using a target-to-substrate distance of 230 mm. The deposition speeds for the In and Li films were approximately 2 and 3 nm s^{-1}, respectively. The synthesis conditions for all layers are summarized in Table 1. The In/Li_3PO_4/Li_2RuO_3 cell cross section was observed by high-angle annular dark-field (HAADF) imaging with a spherical aberration-corrected electron microscope (R005) [22] at 300 kV. The probe beam had a convergent semi-angle of 30 mrad. The inner–outer semi-angle of the HAADF detector was 75–200 mrad. The charge–discharge characteristics of the In/Li_3PO_4/Li_2RuO_3 and the Li/Li_3PO_4/Li_2RuO_3 all-solid-state cells were examined applying a current density of 1.1 μA cm^{-2} and using a probed shield box (Toyo Corporation, Probeh-toy-2) installed in an Ar-filled glove box.

3. Results and discussion

3.1. Film characterization

Fig. 1(a–c) displays the XRD patterns of a 70-nm-thick Li_2RuO_3 film synthesized on Al_2O_3(001). The out-of-plane and in-plane XRD patterns exhibit 00*l* and 060 diffraction peaks based on the monoclinic lattice of the *C*2/*c* space group along Al_2O_3 < 001 > and Al_2O_3 < 100>, respectively. A 6-fold symmetry observed in the ϕ-scan diffraction pattern for the 060 diffraction peak indicates that the Li_2RuO_3(001) film is composed of 60°-rotated domains: Li_2RuO_3[010]//Al_2O_3[100], Li_2RuO_3[010]//Al_2O_3 [1–10], and Li_2RuO_3[010]//Al_2O_3[010] [20]. Weak peaks observed at 41.0° and 59.4° in the out-of-plane and in-plane XRD patterns are attributed to the 400 and 060 RuO_2 reflections with a rutile-type structure [23], indicating the presence of a small amount of RuO_2 as an impurity. The XRD pattern of a 2-μm-thick Li_3PO_4 film on Al_2O_3(001) is shown in Fig. 1d. No diffraction peaks are observed expect for the 00*l* substrate peaks, demonstrating the amorphous character of the Li_3PO_4 film. Fig. 1e summarizes the electrochemical impedance measurement results as an Arrhenius plot. The lithium ion conductivity is 7.0×10^{-7} S cm^{-1} at room temperature with 51 kJ mol^{-1} activation energy, consistent with previously reported values for Li_3PO_4 films [24]. No significant changes in the lattice parameters are observed for the Li_3PO_4-deposited Li_2RuO_3 films.

3.2. Preliminary investigation using a liquid-type cell

Fig. 2 presents the cyclic voltammetry curves obtained from liquid-type cells with the Li_2RuO_3 (001) and 400-nm-thick Li_3PO_4-deposited Li_2RuO_3 (001) film electrodes. The Li_2RuO_3 (001) film shows anodic peaks at 3.5 and 3.7 V and cathodic peaks at 3.3 and 3.6 V. These reaction voltages correspond to lithium (de)intercalation from and in the Li_2RuO_3 lattice [11,12]. The Li_3PO_4-deposited Li_2RuO_3 (001) film exhibits similar redox peaks in the CV curve, although cathodic peaks are slightly shifted to higher voltages. This result indicates lithium diffusion from the Li_2RuO_3 film to the organic electrolyte through the Li_3PO_4 solid electrolyte.

Fig. 3 presents O 1*s* and Ru 3*d*-C 1*s* HAXPES spectra for the 30-nm-thick Li_2RuO_3 (001) and 30-nm-thick Li_3PO_4 deposited Li_2RuO_3 (001) films before and after the electrochemical intercalation

Table 1
Synthesis conditions of each layer.

Target	Method	Energy	Time/h	Distance/mm	Atmosphere	Pressure/Pa	Temperature/°C
LRO	PLD	0.91 mJ cm^{-2}	0.5,1	70	O_2	3.3	500
LPO	Sputtering	100 W	9	30	O_2/Ar	0.48	RT
In	Vapor deposition	60 A/1.37 V	0.5	230	Vacuum	~10^{-3}	RT
Li	Vapor deposition	50 A/0.98V	0.5	230	Vacuum	~10^{-4}	RT

reactions. The peak observed at 530.5 eV for each sample is attributed to the lattice oxygen in the Al_2O_3 substrate, indicating that photoelectrons penetrate through the 30-nm-thick Li_2RuO_3 film due to the high X-ray energy of 8 keV. The HAXPES spectra can provide information concerning the structural changes in the overall region of the Li_2RuO_3 film. The O 1*s*, Ru $3d_{3/2}$, and Ru $3d_{5/2}$ peaks of the pristine Li_2RuO_3 (001) are observed at 529.5, 286.2, and 282.2 eV, respectively (Fig. 3a). These positions are consistent

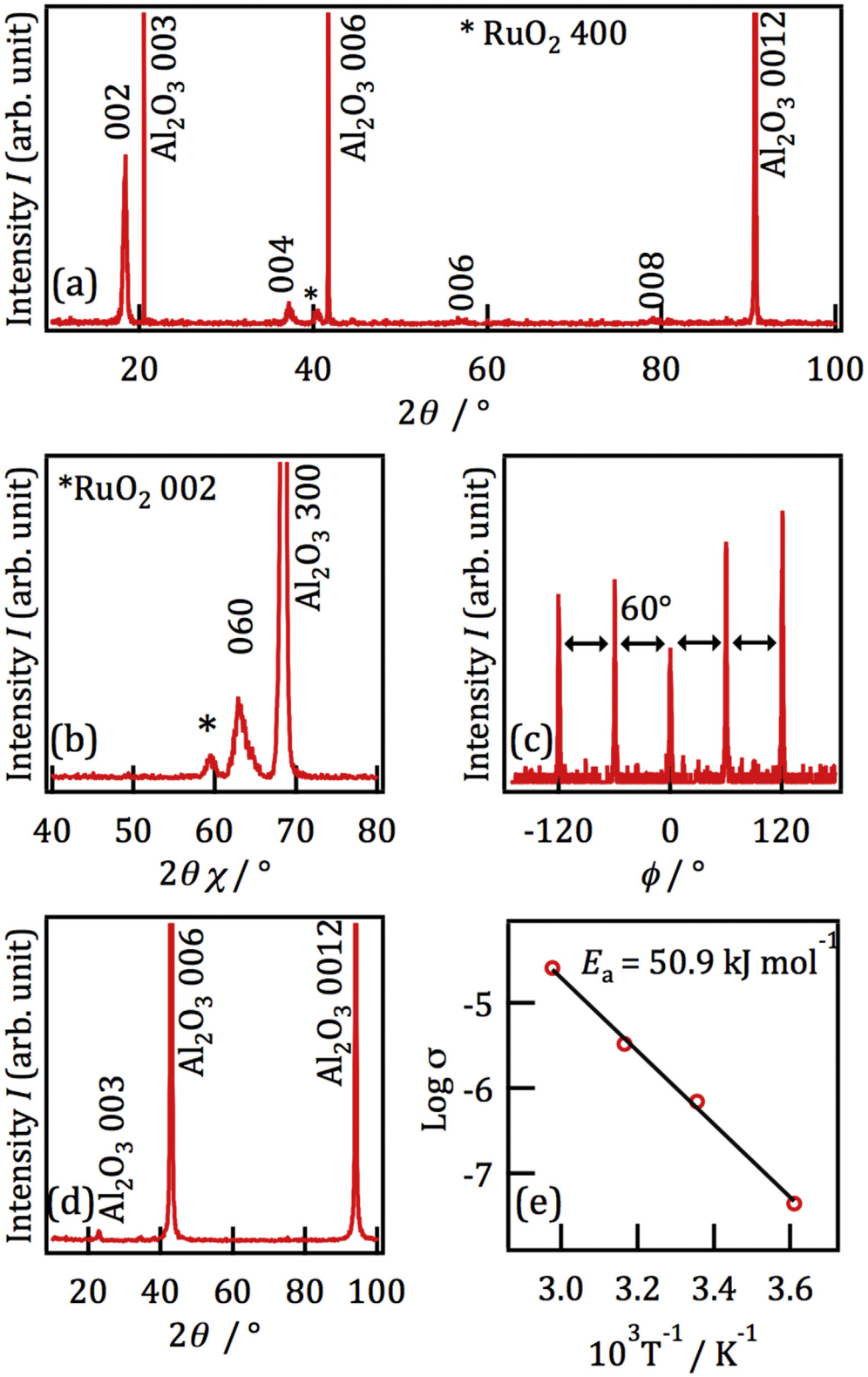


Fig. 1. (a) Out-of-plane and (b,c) in-plane XRD patterns of a 70 nm thick Li_2RuO_3 film deposited on Al_2O_3(0001). (d) Out-of-plane XRD pattern and (e) Arrhenius plot from electrochemical impedance spectroscopy data for a 2 μm thick Li_3PO_4 film on Al_2O_3(0001).

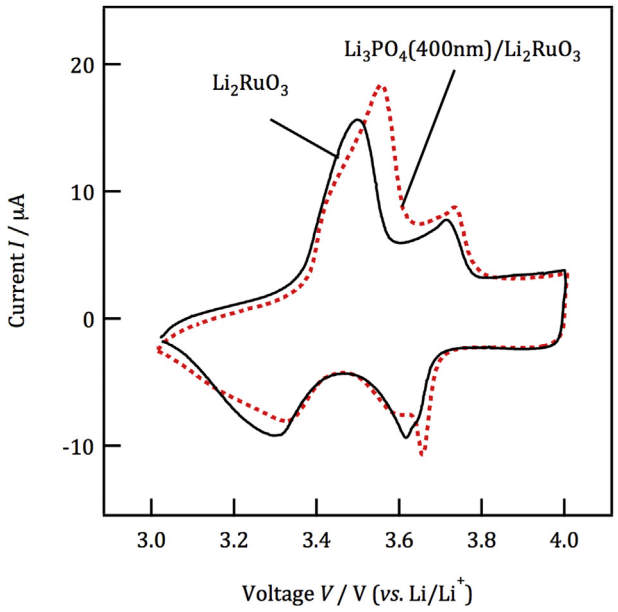


Fig. 2. Cyclic voltammetry plots for Li_2RuO_3 (001) and 400 nm thick Li_3PO_4 deposited on Li_2RuO_3 (001) film cathodes using a liquid-type cell at a scan rate of 0.3 mV s^{-1}.

with values reported previously [25,26]. The presence of carbonate material (285.0 eV) is already visible over most of the film surface, to depths greater than 30 nm [27–29]. Thus, in this study, the formation of multiple carbon species during film deposition is suppressed by the surface-covering method. Although the Li_3PO_4 lattice oxygen peak is observed at 532.5 eV in the Li_3PO_4/Li_2RuO_3 film, no significant changes are noted in the Li_2RuO_3 film at O 1*s* and Ru 3*d* peak positions (Fig. 3b). After the electrochemical reaction, the O 1*s* and Ru 3*d* peaks appear at the same binding energies for both the Li_2RuO_3 and Li_3PO_4/Li_2RuO_3 films, and therefore, there are

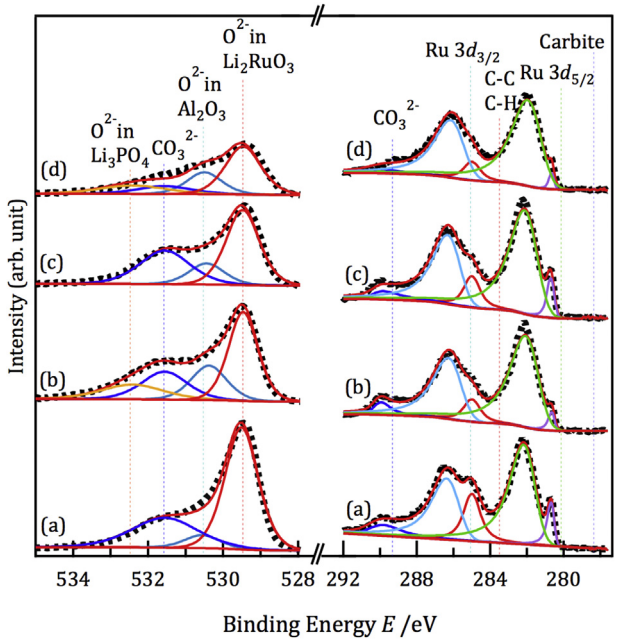


Fig. 3. HAXPES spectra of (a) a pristine Li_2RuO_3 (001) film, (b) 30 nm thick Li_3PO_4 deposited on a Li_2RuO_3 (001) film, (c) the cycled Li_2RuO_3 (001) film, (d) the cycled Li_3PO_4 deposited on a Li_2RuO_3 (001) film (d). The left and right panels show O 1*s* and Ru 3*d*-C 1*s* spectra, respectively.

no significant changes in the electronic states of the oxygen and ruthenium atoms.

3.3. Lithium intercalation properties in all-solid-state batteries

Fig. 4a presents a schematic representation of an assembled all-solid-state battery. The cell is composed of three layers: a P-shaped Li_2RuO_3 cathode layer, larger square Li_3PO_4 electrolyte layer, and reversed P-shaped In anode layer. The reaction surface is 9 mm^2. The STEM image (Fig. 4b) demonstrates that these 3 layers are both dense and flat. The layer thicknesses measured for the cathode Li_2RuO_3, electrolyte Li_3PO_4, and indium layers are 70 nm, 3.1 μm, and 2.0 μm, respectively. The cathode-to-anode molar ratio is 1.7:98.3, calculated using the thickness, deposited area, and theoretical density of the films. The electrochemical properties of the assembled cell are characterized by CV and charge–discharge measurements. Two anodic peaks at 2.9 and 3.2 V, and two cathodic peaks at 2.6 and 2.9 V, are observed in the CV curves (Fig. 4c). At the anodic scan, the formation of an InLi alloy electrochemically proceeded at the anode. Since no solid solution appears at the composition region between In and InLi [30], the lithiation and delithiation ($In + Li^+ + e^- \rightleftarrows InLi$) reversibly proceeded at the Li/Li^+ in the anodic and cathodic scans, as a two-phase reaction at approximately 0.6 V [31]. The potential of the In anode should not change during the charge–discharge processes. Thus, the CV peaks can be attributed to lithium (de)intercalation from or into the Li_2RuO_3 film. The peak separation of the redox peaks is approximately 0.3 V, which is similar to the value determined for Li_2RuO_3 films in a liquid-type cell. These results confirm that lithium intercalation proceeds at the interface between the Li_2RuO_3 cathode and Li_3PO_4 solid electrolyte. The all-solid-state battery exhibits initial charge and discharge capacities of 101.7 and 85.8 mAh g^{-1}, respectively (Fig. 4d), and gradual capacity fading is observed during the initial 10 cycles. The charge–discharge capacities and their cycle stability is smaller than those previously determined for Li_2RuO_3 using liquid-type lithium batteries [10,20]. The lattice volume of the In anode could significantly decrease by 25% at the InLi alloy formation [32], which might decrease the physical contact in the anode material and/or between the anode and the solid electrolyte. Thus, a Li metal anode is investigated to improve the charge–discharge characteristics of the all-solid-state battery.

Fig. 5a presents the charge–discharge plots for a $Li/Li_3PO_4/Li_2RuO_3$ all-solid-state battery in the 3.0–4.0 V voltage range. The Li anode is deposited on the Li_3PO_4/Li_2RuO_3 films synthesized under the same conditions used for the $In/Li_3PO_4/Li_2RuO_3$ film. The all-solid-state battery exhibits clear plateau regions in the charge–discharge curves at approximately 3.4 and 3.6 V, which confirms the lithium intercalation in the Li_2RuO_3 film. The first charge and discharge capacities are 125.8 and 101.4 mAh g^{-1}, respectively, higher than those of the $In/Li_3PO_4/Li_2RuO_3$ cell. Furthermore, no significant capacity fading is observed over 30 cycles. This is consistent with the hypothesis that the Li_2RuO_3 highly reversible lattice change proceeds at the lithium (de)intercalation [23]. Charge–discharge plots in the 2.0–4.0 V voltage range appear in Fig. 5b. Although the curve is similar to that for the 3.0–4.0 V range, another plateau region appears at approximately 2.1 V, which leads to an increase in the charge–discharge capacities of approximately 160 mAh g^{-1}. The excess lithium intercalation in the Li_2RuO_3 proceeds at 1.5 V *vs.* Li/Li^+ [23]. The electrochemical reaction at the 2 V region corresponds to the lithium intercalation into a rutile-type RuO_2 phase detected by XRD (Fig. 1) [33]. The RuO_2 phase incorporation decreases the charge–discharge capacities of the $Li/Li_3PO_4/Li_2RuO_3$ and $In/Li_3PO_4/Li_2RuO_3$ cells between 3.0 and 4.0 V (vs. Li/Li^+), because there is no electrochemical activity of the rutile-type RuO_2 above 3 V [33].

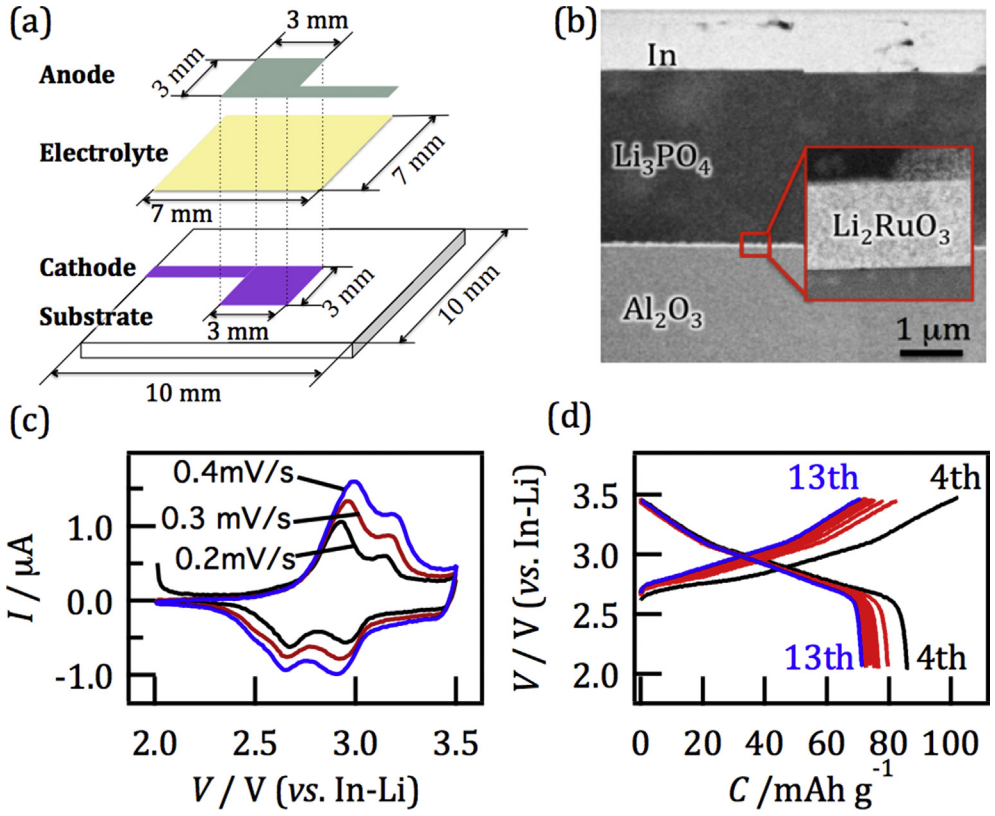


Fig. 4. (a) Schematic of the cell design, (b) STEM image of the device cross-section, (c) CV plots at scan rates of 0.2–0.4 mV s^{-1} and (d) charge/discharge plots collected at 1.1 μA cm^{-2} for an In/Li_3PO_4/Li_2RuO_3 all-solid-state battery.

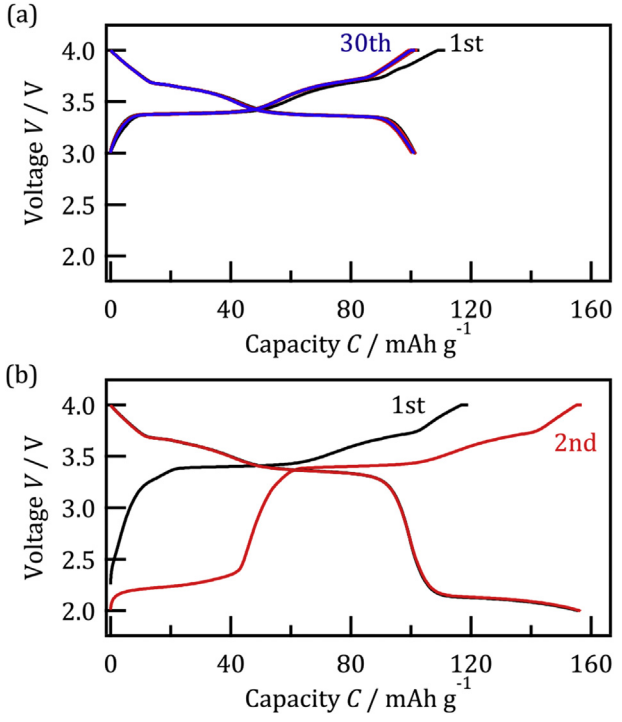


Fig. 5. Charge/discharge plots collected under 0.1 C operation for Li/Li_3PO_4/Li_2RuO_3 all-solid-state batteries in voltage ranges of (a) 3.0 V–4.0 V and (b) 2.0 V–4.0 V.

Fig. 6 presents variations in the discharge capacity retentions of the Li/Li_3PO_4/Li_2RuO_3 cell depending on the cycle number and the C rate. The cycle retention of the cell operated at 0.1 C (1.67 μA cm^{-2}) was examined during the initial 30 cycles, and then the current densities increased every 5 cycles from 0.1 C to 0.5 C, 1 C, 2C, 5 C, 10 C, 20 C. The discharge capacity significantly decreases over 2 C, to 87 mAh g^{-1}, 80 mAh g^{-1}, and 63 mAh g^{-1} for 5 C, 10 C, and 20 C, respectively. The discharge capacity at 20 C is 63% of the capacity at 0.1 C. The capacity retention at the different C rates is comparable to that of the Li_2RuO_3(001) film characterized using a liquid-type cell

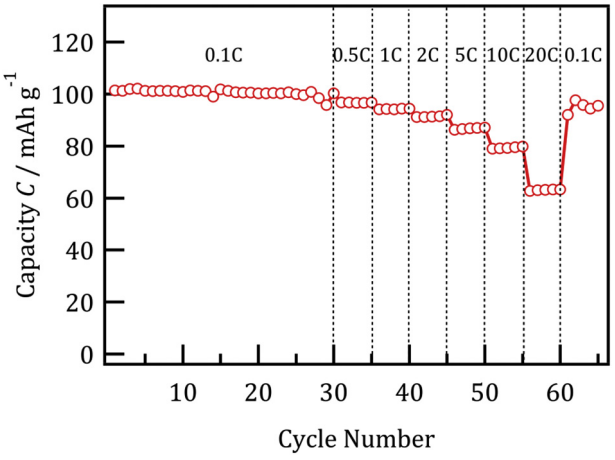


Fig. 6. Variations in discharge capacity retention of a Li/Li_3PO_4/Li_2RuO_3 all-solid-state battery with cycle number and charge/discharge C rates. The voltage range was 3.0 V–4.0 V.

of Li_2RuO_3(001)/organic electrolyte/Li; the latter exhibited a discharge capacity at 20 C that was 58% of that at 0.5 C [23]. The lithium intercalation proceeds at the solid–solid interface as well as the solid–liquid interface within the range of the current density examined in this study. This result indicates that the homogeneous solid–solid interface formed on the film electrode provides a reaction plane suitable for lithium intercalation.

Our results provide the first example of an all-solid-state battery incorporating a lithium-rich layered rocksalt oxide cathode and an oxide solid electrolyte. The cycle performance and the rate capability of the Li_2RuO_3 cathode are comparable to those of the $LiCoO_2$ cathode in all-solid-state batteries [34]. The lithium-rich layered rocksalt oxide system could expand the application of cathode materials in high capacity all-solid-state batteries.

4. Summary

A solid–solid interface between a Li_2RuO_3 (001) cathode and an amorphous Li_3PO_4 electrolyte is obtained by PLD and RF sputtering. The epitaxial Li_2RuO_3 (001) film cathode shows lithium intercalation activity through the solid–solid interface with reversible changes in the oxidation state of the Ru atoms. An all-solid-state Li_2RuO_3/Li_3PO_4/In battery with no current collector layer exhibits initial charge and discharge capacities of 101.7 and 85.8 mAh g^{-1}, respectively. The all-solid-state battery with a Li metal anode exhibits a higher discharge capacity of 101.4 mAh g^{-1} and no significant capacity fading over 30 cycles. The rate capability of the Li_2RuO_3/Li_3PO_4/Li battery is comparable to that of a liquid-type battery with an organic electrolyte. The lithium-rich layered rocksalt oxides are promising cathode materials for high capacity all-solid-state batteries.

Acknowledgments

This study was partly supported by a Grant-in-Aid from the Advanced Low Carbon Technology Research and Development Program (ALCA) of the Japan Science and Technology Agency (JST). The research was also partly supported by a Grant-in-Aid for Scientific Research (A) (no. 25248051) and a Grant-in-Aid for Scientific Research (C) (no. 25410237) from the Japan Society for the Promotion of Science. The synchrotron experiments were performed with the approval of the Japan Synchrotron Radiation Research Institute (JASRI) (proposal no. 2011A1734).

References

[1] S. Jones, J. Akridge, J. Power Sources 54 (63) (1995) 63–67.
[2] J.D. Wang, B. Bates, J.B. Hart, F.X. Sales, B.C. Zuhr, R.A. Roberson, J. Electrochem. Soc. 143 (1996) 3203–3213.
[3] Y.-I. Jang, N.J. Dudney, D.A. Blom, L.F. Allard, J. Electrochem. Soc. 149 (2002) A1442–A1447.
[4] H.-K. Kim, T.-Y. Seong, Y.-S. Yoon, Electrochem. Solid State Lett. 5 (2002) A252–A255.
[5] R. Baskaran, N. Kuwata, O. Kamishima, J. Kawamura, S. Selvasekarapandian, Solid State Ionics 180 (2009) 636–643.
[6] J.B. Bates, N.J. Dudney, D.C. Lubben, G.R. Gruzalski, B.S. Kwak, X. Yu, R.A. Zuhr, J. Power Sources 54 (1995) 58–62.
[7] Y. Park, S. Lee, B. Lee, S. Joo, Electrochem. Solid State Lett. 2 (1999) 58–59.
[8] J.-Z. Wang, S.-L. Chou, J. Chen, S.-Y. Chew, G.-X. Wang, K. Konstantinov, J. Wu, S.-X. Dou, H.K. Liu, Electrochem. Commun. 10 (2008) 1781–1784.
[9] K. Iwamoto, N. Aotani, K. Takada, S. Kondo, Solid State Ionics 70/71 (1994) 658–661.
[10] H. Kobayashi, R. Kanno, Y. Kawamoto, M. Tabuchi, O. Nakamura, M. Takano, Solid State Ionics 82 (1995) 25–31.
[11] H. Kobayashi, R. Kanno, Y. Kawamoto, M. Tabuchi, O. Nakamura, Solid State Ionics 86–88 (1996) 859–863.
[12] H. Kobayashi, R. Kanno, M. Tabuchi, H. Kageyama, O. Nakamura, M. Takano, J. Power Sources 68 (1997) 686–691.
[13] K. Asakura, S. Okada, H. Arai, S.-i. Tobishima, Y. Sakurai, J. Power Sources 81–82 (1999) 388–392.
[14] D. Mori, H. Sakaebe, M. Shikano, H. Kojitani, K. Tatsumi, Y. Inaguma, J. Power Sources 196 (2011) 6934–6938.
[15] Z. Lu, L.Y. Beaulieu, R.A. Donaberger, C.L. Thomas, J.R. Dahn, J. Electrochem. Soc. 149 (2002) A778–A791.
[16] Y.M. Todorov, K. Numata, Electrochim. Acta 50 (2004) 495–499.
[17] K. Shizuka, T. Kobayashi, K. Okahara, K. Okamoto, S. Kanzaki, R. Kanno, J. Power Sources 146 (2005) 589–593.
[18] M.M. Thackeray, S.H. Kang, C.S. Johnson, J.T. Vaughey, S.A. Hackney, Electrochem. Commun. 8 (2006) 1531–1538.
[19] S. Sarkar, P. Mahale, S. Mitraz, J. Electrochem. Soc. 161 (2014) A934–A942.
[20] Y. Zheng, S. Taminato, K. Suzuki, M. Hirayama, R. Kanno, Thin Solid Films 520 (2012) 4889–4893.
[21] Y. Zheng, S. Taminato, Y. Xu, K. Suzuki, K. Kim, M. Hirayama, R. Kanno, J. Power Sources 208 (2012) 447–451.
[22] H. Sawada, Y. Tanishiro, N. Ohashi, T. Tomita, F. Hosokawa, T. Kaneyama, Y. Kondo, K. Takayanagi, J. Electron. Microsc. 58 (6) (2009) 357.
[23] S. Taminato, M. Hirayama, K. Suzuki, K. Kim, Y. Zheng, K. Tamura, J. Mizuki, R. Kanno, J. Mater. Chem. 2 (2014) 17875–17882.
[24] N. Kuwata, J. Kawamura, K. Toribami, Electrochem. Commun. 6 (2004) 417–421.
[25] M. Sathiya, K. Ramesha, G. Rousse, D. Foix, D. Gonbeau, a S. Prakash, M.L. Doublet, K. Hemalatha, J.-M. Tarascon, Chem. Mater. 25 (2013) 1121–1131.
[26] M. Sathiya, G. Rousse, K. Ramesha, C.P. Laisa, H. Vezin, M.T. Sougrati, M.-L. Doublet, D. Foix, D. Gonbeau, W. Walker, a S. Prakash, M. Ben Hassine, L. Dupont, J.-M. Tarascon, Nat. Mater. 12 (2013) 827–835.
[27] K.S. Kim, N. Winograd, J. Catal. 35 (1974) 66.
[28] J.Y. Shen, A. Adnot, S. Kaliaguine, Appl. Surf. Sci. 51 (1991) 47–60.
[29] Y. Wu, H.-S. Tao, E. Garfunkel, T.E. Madey, N.D. Shinn, Surf. Sci. 336 (1995) 123–139.
[30] J. Sangster, A.D. Pelton, J. Phase Equilib. 12 (1991) 37–41.
[31] Y.S. Jung, K.T. Lee, J.H. Kim, J.Y. Kwon, S.M. Oh, Adv. Funct. Mater. 18 (2008) 3010–3017.
[32] W.A. Alexander, L.D. Calvert, R.H. Gamble, K. Schinzel, Can. J. Chem. 54 (1976) 1052–1060.
[33] T. Ohzuku, K. Sawai, T. Hirai, J. Electrochem. Soc. 137 (1990) 3004–3010.
[34] S. Tintignac, R. Baddour-Hadjean, J.P. Pereira-Ramos, R. Salot, Electrochim. Acta 146 (2014) 472–476.